The multimethod palaeointensity approach applied to volcanics from Terceira: full-vector geomagnetic data for the past 50 kyr

Lennart V. de Groot,[1] Adriano Pimentel[2,3] and Anita Di Chiara[4]

[1]*Paleomagnetic Laboratory Fort Hoofddijk, Department of Earth Sciences, Faculty of Geosciences, Utrecht University, Utrecht, The Netherlands.*
E-mail: l.v.degroot@uu.nl
[2]*Centro de Vulcanologia e Avaliação de Riscos Geológicos, Universidade dos Açores, Rua Mãe de Deus, 9501–801 Ponta Delgada, Azores, Portugal*
[3]*Centro de Informação e Vigilância Sismovulcânica dos Açores, Rua Mãe de Deus, 9501–801 Ponta Delgada, Azores, Portugal*
[4]*Departamento de Geofísica, Instituto de Astronomia, Geofísica e Ciências Atmosféricas–Universidade de São Paulo, Rua do Matão, 1226, 05508090, Cidade Universitária, São Paulo, SP, Brasil*

SUMMARY

The island of Terceira (38.5°N, 27.2°W) in the Azores Archipelago boasts a wealth of well-dated recent volcanic products; it is therefore the ideal location to improve the resolution of the full-vector geomagnetic field record for the Mid-Atlantic Ocean. We investigated 21 (sub-)sites sampled from 10 different cooling units; six of these cooling units are from the Holocene, the other four are approximately coeval with the age of known geomagnetic excursions. After successfully determining the palaeodirections from all but one site, we applied the multimethod palaeointensity approach to all sites. Here, we used three different palaeointensity methods: the IZZI-Thellier protocol, the Multispecimen technique, and the calibrated pseudo-Thellier method. For the Holocene sites four robust palaeointensity estimates were obtained, they mostly agree with data from the nearby island of São Miguel and data from the Iberian Peninsula and West Africa. Two older sites, dated at 25.7 and 46.3 ka, produced low palaeointensities: 24.4 and 24.1 μT, respectively. As both the IZZI-Thellier and pseudo-Thellier methods yielded technically acceptable results for these sites we used them to improve the pseudo-Thellier calibration relation and establish its applicability to lower palaeointensities. Sixty per cent of all sampled cooling units/ages in our study yielded a technically successful palaeointensity estimate; this unusually high success rate is attributed both to our sampling strategy and the implementation of the multimethod approach.

Key words: Geomagnetic excursions; Palaeointensity; Palaeomagnetic secular variation; Rapid time variations; Atlantic Ocean.

1 INTRODUCTION

Our understanding of the behaviour of the geomagnetic field critically depends on the availability and quality of full-vector data and their variations (e.g. Nilsson *et al.* 2014; Pavón-Carrasco *et al.* 2014). Currently available data are considerably biased towards certain regions of the Northern Hemisphere: Europe, some parts of North America and Japan are overrepresented. Attaining a more global coverage is paramount to improving the quality of the geomagnetic models. The Azores Archipelago is located in the middle of the Atlantic Ocean; its volcanic products therefore record the behaviour of the geomagnetic field in a remote area that otherwise is uncovered. Recently, Di Chiara *et al.* (2012) produced secular variation data for the Azorean island of São Miguel, and Di Chiara *et al.* (2014) were the first to produce a coherent set of palaeointensity data for that same island. Here, we aim to improve the resolution of the full-vector geomagnetic record for the Azores region. The island

of Terceira (38.5°N, 27.2°W) hosts a wealth of well-dated volcanic products that are suitable to determine both palaeodirections and palaeointensities.

Obtaining a reliable palaeodirection from lava flows is quite straightforward; averaging the directions of several independently oriented samples usually yields a reliable estimate of the declination and inclination of the palaeofield. By contrast, producing reliable estimates of the palaeofield's intensity from volcanic samples is—despite significant methodological progress over the past decades—notoriously challenging. The IZZI-Thellier method (Tauxe & Staudigel 2004) arguably is the most used palaeointensity method today. It results from more than 50 yr of development since Thellier and Thellier first published their palaeointensity results (Thellier & Thellier 1959). Various checks, such as pTRM-checks (Coe 1967) and pTRM-tail-checks (Riisager & Riisager 2001) are used to assess the quality of the measurements, and results are routinely scrutinized with various sets of selection criteria such as

SELCRIT-1 (Selkin & Tauxe 2000), PICRIT-03 (Kissel & Laj 2004) and TTA & TTB (Leonhardt *et al.* 2004). The performance of those selection criteria was recently tested by Paterson *et al.* (2014) and some refinements were proposed. Other methods to obtain reliable estimates of the palaeofield were also put forward: the usage of microwaves to directly excite the samples' magnetic system was found to be useful in reducing the thermally induced alteration that many volcanic samples exhibit during classical Thellier experiments (Hill & Shaw 1999, 2000). Taking a different thermal approach, Dekkers & Böhnel (2006) proposed a method exploiting multiple sister specimens and reducing the number of heating steps compared to Thellier-style protocols. This multispecimen method (MSP) was later refined by Fabian & Leonhardt (2010) to account for potential changes in the magnetic domain state during the experiment. To avoid thermally induced alteration altogether, a relative palaeointensity technique frequently used on sediments, the pseudo-Thellier method, was recently calibrated to provide absolute estimates of the palaeofield's intensity from volcanic samples and proved to be a valuable addition to the palaeointensity toolbox (de Groot *et al.* 2013).

The number of reliable palaeointensity estimates arising from a single study can be increased by (1) sampling cooling units at various locations and/or at different depths in the unit (de Groot *et al.* 2014) and (2) implementing several of the aforementioned palaeointensity techniques in one study (de Groot *et al.* 2013, 2015). Studies adopting this approach yielded reliable estimates of the palaeofield's intensity for 60–70 per cent of all possible flows/ages

in their data sets, contrasting with the success rate of ∼20 per cent for classical intensity approaches (e.g. Valet 2003). Here we apply the IZZI-Thellier, MSP and calibrated pseudo-Thellier techniques to a set of samples taken at various locations from 10 well-dated volcanic units on the island of Terceira (Azores). Six flows are from the Holocene, the other four units are considerably older: 25.7, 46.3, 116.3 and 401 ka. The Holocene flows will add to the current full-vector curves of secular variation in the Azores region (Di Chiara *et al.* 2012, 2014). The youngest three of the older units are (nearly) coeval to known excursions of the geomagnetic field: the Mono Lake, Laschamps and Blake events, respectively, and may therefore shed light on the expression of these events in this remote region of the Mid-Atlantic.

2 GEOLOGICAL SETTING AND SAMPLING STRATEGY

Terceira (38.5°N, 27.2°W) is one of the nine islands comprising the Azores Archipelago (Portugal), which straddles the Northern Mid-Atlantic ridge. The island emerged during the Pleistocene (Calvert *et al.* 2006; Hildenbrand *et al.* 2014) and is composed of four central volcanoes and a fissure zone, which extends diagonally across the island along a broad WNW–ESE orientation (Fig. 1, e.g. Self 1976; Calvert *et al.* 2006; Gertisser *et al.* 2010; Quartau *et al.* 2014; Zanon & Pimentel 2015). The oldest volcano of Terceira is Cinco Picos (>401 ka; Hildenbrand *et al.* 2014) that together with Guilherme
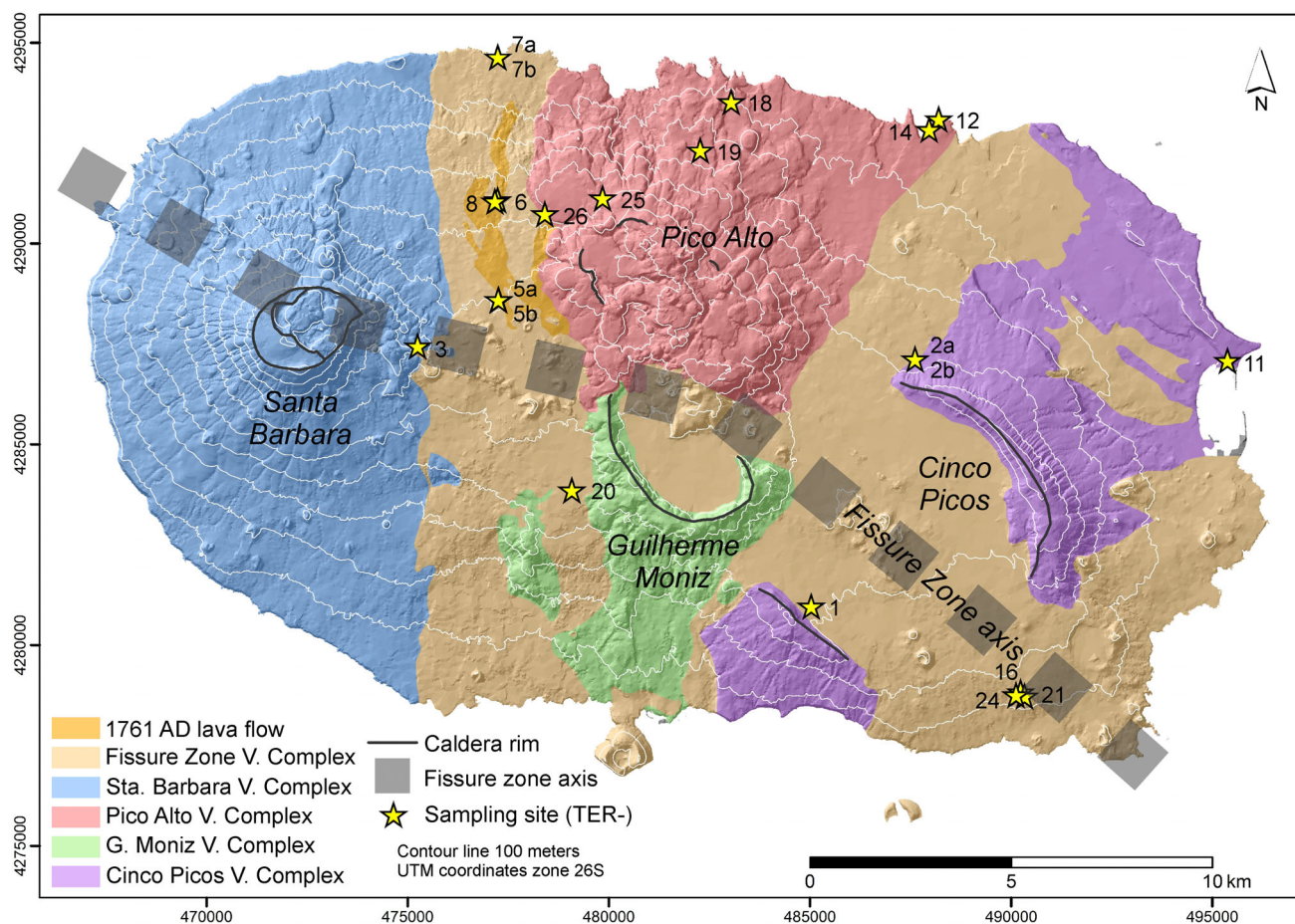
Figure 1. Simplified geological map of Terceira Island (modified from Madeira 2005). Yellow stars indicate the sampling sites. The four volcanic complexes are older towards the east and younger towards the west; the most recent volcanic activity is found in the fissure zone. Map coordinates are in UTM, zone 26S.

Table 1. Site details. For all sampled sites the following information is provided: the name of the unit, site number, location in UTM coordinates (zone 26S), its age as provided (laboratory age for the ^{14}C datings), the nature of the age constraint (^{14}C, radiocarbon; pmag, palaeomagnetically constrained; historical, constrained based on historical observations; Ar/Ar, argon–argon radiometrically dated); the calibrated radiocarbon age (if applicable) after calibration with the INTCAL.13 curve, and the literature reference (ref.) of the dating (A, Calvert *et al.* 2006; B, Pimentel *et al.* 2016; C, Hildenbrand *et al.* 2014). Sites are grouped per unit, if multiple sites are taken from the same cooling unit, the same dating applies.

Unit	Site (TER-)	Location	Age	Age constraint	Calibrated radiocarbon age [AD]	Ref.
Algar do Carvao	1	26 S 0485027; UTM 4280975	1910 ± 35 BP	^{14}C	94 [59−128, 1.000]	A
”	2a	26 S 0487609; UTM 4287127				
”	2b	26 S 0487609; UTM 4287127				
Misterios Negros	3	26 S 0475247; UTM 4287453	1761 AD	pmag		B
1761 flow	5a	26 S 0477264; UTM 4288598	1761 AD	historical		–
”	5b	26 S 0477253; UTM 4288603				
”	6	26 S 0477234; UTM 4291096				
Pico Gordo	7a	26 S 0477242; UTM 4294646	4480 ± 40 BP	^{14}C	−3210 [−3332 to −3214, 0.657; −3187 to −3156, 0.162; −3129 to −3095, 0.181]	A
”	7b	26 S 0477242; UTM 4294646				
”	8	26 S 0477171; UTM 4291056				
Praia lower	11	26 S 0495377; UTM 4287092	401 ± 6 ka	Ar/Ar		C
Vila Nova lower	12	26 S 0488201; UTM 4293102	116.3 ± 1.6 ka	Ar/Ar		A
Lajes ignimbrite	14	26 S 0487963; UTM 4292845	21,320 ± 80 BP	^{14}C	−23718 (25.7 ka) [−23819 to −23628, 1.000]	A
Porto Judeu	16	26 S 0490232; UTM 4278838	43,020 ± 740 BP	^{14}C	−44323 (46.3 ka) [−45003 to −43552, 1.000]	A
”	21	26 S 0490331; UTM 4278735				
”	24	26 S 0490119; UTM 4278768				
Pico Alto	18	26 S 0483042; UTM 4293529	1,760 ± 40 BP	^{14}C	283 [141 to 160, 0.031; 165 to 196, 0.058; 209 to 384, 0.911]	A
”	19	26 S 0482272; UTM 4292329				
Vareiras	20	26 S 0479081; UTM 4283866	10,090 ± 50 BP	^{14}C	−9719 [−9862 to −9651, 0.803; −9601 to −9545, 0.151; −9481 to −9462, 0.046]	A
Pardelas	25	26 S 0479845; UTM 4291134	8,670 ± 50 BP	^{14}C	−7673 [−7713 to −7601, 1.000]	A
”	26	26 S 0478407; UTM 4290742				

Moniz volcano (>270 ka; Calvert *et al.* 2006) are considered extinct. The two youngest volcanoes, Pico Alto (>141 ka; Gertisser *et al.* 2010) and Santa Barbara (>65 ka; Hildenbrand *et al.* 2014), are active and have erupted contemporaneously with the fissure zone, at least in the last 50 ka. The most recent subaerial volcanic activity was in the fissure zone in the centre of the island, where the last eruption occurred in 1761 AD (Self 1976; Calvert *et al.* 2006; Zanon & Pimentel 2015). Lavas from the fissure zone are mainly basaltic, while the volcanic products of the four central volcanoes range from basaltic to trachytic and rhyolitic.

During our sampling campaign we sampled 18 sites throughout the island of Terceira from 10 different cooling units with a good age control (Fig. 1); 12 of those are from the Holocene (six ages), the other six were emplaced earlier in the Brunhes chron (four ages; Table 1). Of these 19 sites, two sites are from the historical 1761 AD lava flow, one is palaeomagnetically dated to have that same age (Pimentel *et al.* 2016); 13 were sampled from radiocarbon-dated volcanic units (Calvert *et al.* 2006); the last two are taken from lava flows that were dated by argon–argon by (Calvert *et al.* 2006) and (Hildenbrand *et al.* 2014; Table 1). The majority of age constraints for our study are provided by radiocarbon dates (Calvert *et al.* 2006). Inherently, this technique does not date the rock itself, but exploits traces of burnt carbon (i.e. wood, shrubs, etc.) associated with the volcanic products. Nevertheless, the carbon

considered for dating generally is well embedded or even enclosed in the deposits, increasing the robustness of its correlation to the age of the units, and therefore the reliability of these age constraints (Calvert *et al.* 2006). The radiocarbon ages were recalibrated with the latest INTCAL.13 curve (Reimer *et al.* 2013) using the Calib 7.0 website (Stuiver & Reimer 1993; Table 1). The sampled units are mostly basaltic lava flows, except for three (sites 3, 18, 19, 25 and 26) that are trachytic in composition, while site 14 corresponds to a welded trachytic ignimbrite.

At each site we took a number of samples as close together as possible (1–5 cm apart) to ensure among sample homogeneity to compare the palaeointensity results. Furthermore we took seven to eight samples up to 10 m apart at various parts of the outcrop to obtain a reliable palaeodirection, this latter group of samples is referred to as the 'X-samples'. At sites 2, 5 and 7 two groups of samples (a and b) were taken up to 10 m apart, because of variation in the physical appearance of the lava. Standard palaeomagnetic cores (2.5 cm in diameter, up to 10 cm in length) were taken using a petrol-powered drill. Whenever possible the cores were oriented using both a magnetic and a sun compass; the difference in the obtained orientation was generally very small and always <5°. The top of the cores was routinely discarded because of possible weathering of the surface of the outcrops. A kml-file with our sampling locations is provided in the supplementary information.

Table 2. Rock-magnetic characterization and palaeodirections. Per site the following rock-magnetic parameters are specified: the name of the unit, the site number, the rock-magnetic group (see main text), the room temperature (RT) susceptibility, the dominant Curie temperature (Dom. Curie *T.*), and the alteration temperature (Alt. *T.*). The directions are given at site and age group level: the declination (dec), inclination (inc), 95 per cent confidence interval (α_{95}), precision parameter (*k*), and the number of samples interpreted (*N*, with the amount of samples rejected by a 45° cut-off between brackets). The directions of sites 3, 5 and 6 (marked with an ∗) were published before in Pimentel *et al.* (2016).

Unit	Site (TER-)	Rock mag. group	RT susc. $\times 10^6$ (m^3 kg^{-1})	Dom. Curie *T.* (°C)	Alt. *T.* (°C)	Per site					Per unit				
						Dec (°)	Inc (°)	α_{95} (°)	*k*	*N* (rej.)	Dec (°)	Inc (°)	α_{95} (°)	*k*	*N* (rej.)
Algar do Carvao	1	M*	11.9	100/490	370	−10.9	56.3	4.8	102.8	10	−2.8	54.5	3.2	84.9	24
"	2a	H	4.31	260/550	320	2.4	52.9	3.9	107.3	14					
"	2b	H	4.87	550	320										
Mistérios Negros (1761)	3*	M	1.40	gradual >300	none	−24.9	68.8	4.7	104.5	10					
"	4	M	0.903	190/330	320	−	−	−	−	−					
1761 flow	5a*	M	2.31	240/550	200	−24.1	68.3	5.4	79.8	14 (4)	−22.4	67.7	2.5	117.1	34 (5)
"	5b*	M	2.30	160	320										
"	6*	L	5.71	100	320	−18.2	65.8	3.0	291.7	10 (1)					
Pico Gordo	7a	H	11.0	560	320	−8.1	51.7	4.4	61.5	18 (1)	−8.5	53.7	3.4	66.8	27 (2)
"	7b	H	3.58	560	280										
"	8	H	13.5	560	320	−9.6	57.8	5.1	101.5	9 (1)					
Praia lower	11	H	12.5	550	320	−5.6	16.7	2.7	429.5	8					
Vila Nova lower	12	H	4.60	200/520	200	−	−	−	−	−					
Lajes ignimbrite	14	H	1.43	560	320	−23.8	57.2	2.6	343.7	10					
Porto Judeu	16	H	9.48	550	370	−12.6	56	6.7	60.7	9	−9.3	54.0	4.5	52.6	21 (1)
"	21	H	11.6	540	320	−10.6	51.4	11.6	34.1	6					
"	24	H	11.8	500	430	−2.0	53.3	8.7	78.0	5 (1)					
Pico Alto	18	M*	0.556	gradual >400	580	−4.9	42.6	8.7	31.6	10	−2.5	42.9	4.4	56.7	20
"	19	H	0.617	540	320	0.0	43.2	3.3	221.6	10					
Vareiras	20	H	16.1	540	320	−17.3	57.6	12.1	31.7	6					
Pardelas	25	M	1.14	140/500	320	−	−	−	−	−					
"	26	M	1.15	220/550	320	41.6	35.6	5.8	71.1	10					

3 ROCK-MAGNETIC BEHAVIOUR

To optimize palaeointensity experiments samples from all sites are first subjected to a number of rock-magnetic analyses; both low- and high-field measurements were performed. The low-field susceptibility is analysed as function of temperature using an AGICO KLY-3S susceptometer with a CS3 furnace attachment. The temperature was increased in seven cycles with approximate peak temperatures of 210, 280, 330, 375, 430, 480 and 580 °C; after each peak the temperature was lowered at least 50 °C to check for alteration: the occurrence of an irreversible segment indicates chemical alteration in the sample. The highest temperature with reversible susceptibility behaviour is the highest temperature that can safely be used in palaeointensity experiments and is referred to as 'alteration temperature' (Table 2). The Curie temperature can also be derived from the susceptibility versus temperature analyses (Petrovský & Kapička 2006); the inflection point after a peak in susceptibility can be interpreted as such. Seven sites show two distinct Curie temperatures; two sites exhibit a very gradual decay in susceptibility with temperature, therefore a distinct Curie temperature cannot be determined (Table 2).

The high-field magnetic properties of the samples is characterized by a Day-plot (Day *et al.* 1977; Dunlop 2002). The necessary parameters [the saturation magnetization (M_s), remanent saturation magnetization (M_r), coercive field (B_c) and remanent coercive field

(B_{cr})] were measured on a Princeton PMC 2900 alternating gradient force magnetometer. Per site, the measurements of three small samples (2–10 mg) were normalized to their mass and averaged to obtain reliable estimates from the heterogeneous bulk samples. For sites with large uncertainties another three samples were measured to decrease the confidence intervals. The differences in uncertainty between the sites possibly arise from heterogeneities in the sample material: since the samples are very small samples from coarse-grained lavas may not represent the properties of the bulk samples fully. Why the uncertainties in the coercivity ratio are notably larger than the errors in the squareness (e.g. sites 3, 25 and 26) is not fully understood. Most sites are close to the theoretical SD+MD mixing lines for coarse and fine grained end members (Dunlop 2002; Fig. 3). Site 5b is in the SD realm, the rest of the sites are within the PSD region of the Day-plot.

All sites are divided in rock magnetic groups based on the behaviour of their susceptibility as function of temperature. The groups are akin to those used in de Groot *et al.* (2015).

3.1 Group L

Group L consists of samples that lose more than 80 per cent of their room temperature susceptibility below 150 °C (Fig. 2a). In this study, only site 6 shows this behaviour. Although samples of
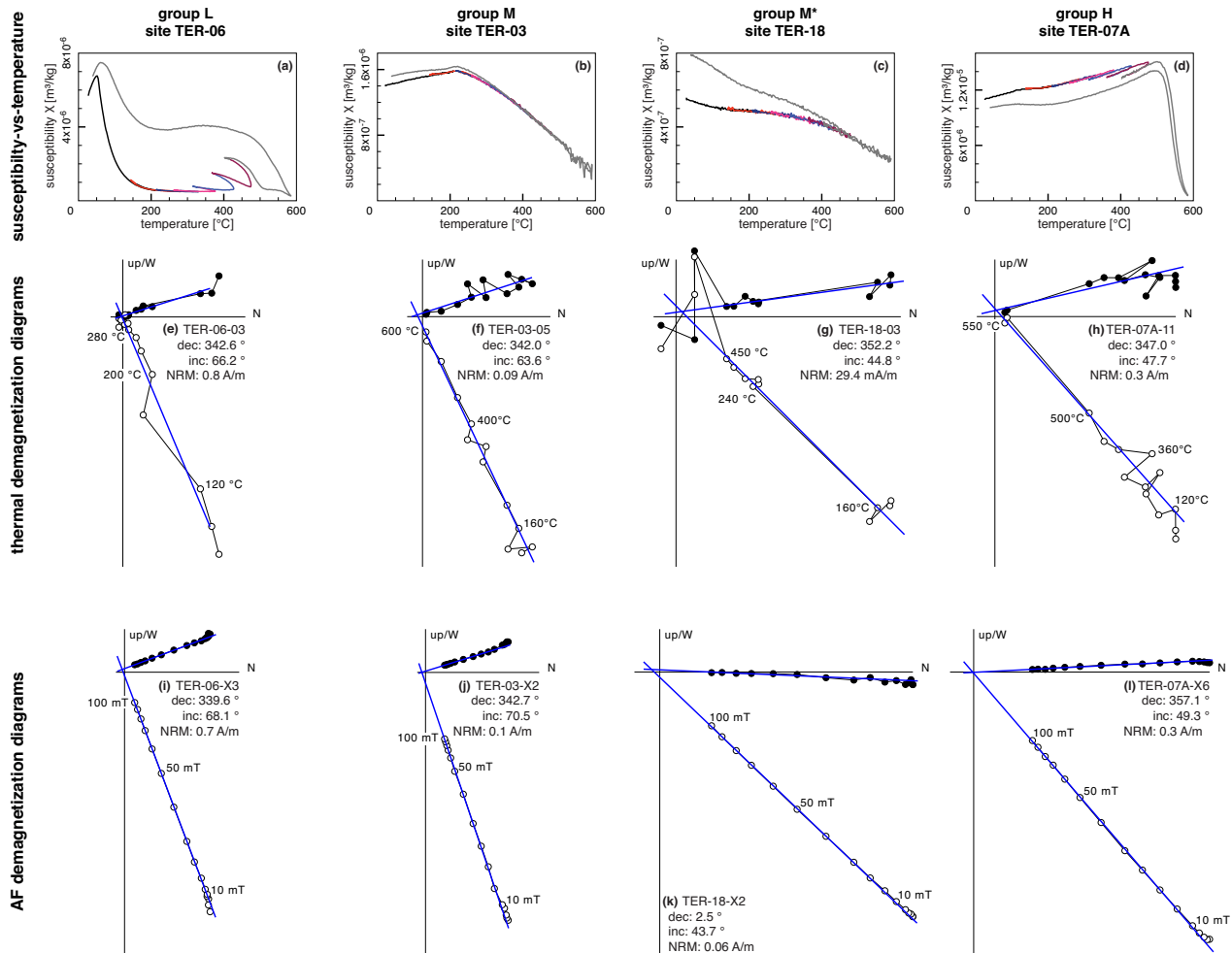
Figure 2. Rock-magnetic characterization. For each rock-magnetic group (see main text) examples of susceptibility behaviour as function of temperature (a–d), thermal demagnetization (e–h), and AF demagnetization (i–l) are given. In the susceptibility versus temperature diagrams (a–d), temperature segments are depicted with different colours, the last thermal cycle and the final cooling curve is in grey. The noise in the measurements [higher temperatures TER-03 (b) and TER-18 (c)] are due to the low susceptibility values. In the Zijderveld diagrams (e–l) the obtained direction [declination (dec)/inclination (inc)] and the NRM intensity (NRM) are specified, as are some characteristic temperature steps. The blue lines are the interpreted directions.

site 6 might be vulnerable to viscous overprints, these are very small. At 280 °C less than 5 per cent of the NRM remains in the samples (Fig. 2e). In the Day-plot site six plots near theoretical SP+SD mixing line, indicating a relatively large contribution of very small superparamagnetic grains (Day *et al.* 1977; Dunlop 2002; Fig. 3).

3.2 Group M

Samples in group M (sites 3, 4, 5a, 5b, 25 and 26) retain more than 20 per cent of their room temperature susceptibility at 150 °C, but lose more than 20 per cent of it before reaching 400 °C (Fig. 2b). Within this group there is no distinction between sites with a gradually decay in susceptibility, or sites with two or more distinct Curie temperatures. The high-field rock magnetic behaviour of samples in group M is not coherent: site 5b plots in the SD realm of the Day-plot, while sites 3, 25 and 26, are closest to MD behaviour in our Terceira collection (Fig. 3). Group M samples generally demagnetize gradually between 100 and 600 °C (Fig. 2f).

3.3 Group M*

Sites 1 and 18 form group M*, they fulfil the criteria of group M, but their susceptibility decays from room temperature onwards, implying a Hopkinson peak below room temperature (Fig. 2c). These samples may therefore be prone to viscous behaviour at or just above room temperature; as palaeointensities can only be trusted if the directions are stable during the experiments and trend towards the origin, samples from this rock-magnetic group have to be checked in particular for consistent directional behaviour. Sites 1 and 18 are both well within the PSD realm of the Day-plot (Fig. 3). The NRMs of site 18 are 1–2 orders of magnitude lower than samples from other sites, the directions in these samples are stable during demagnetization up to 450 °C and deteriorate for higher temperatures (Fig. 2g); it is noteworthy that the susceptibility of this site also is reversible up to ~450 °C and increases irreversibly for higher temperatures.

3.4 Group H

Samples in group H (sites 2a, 2b, 7a, 7b, 8, 11, 12, 14, 16, 19, 20, 21 and 24) preserve more than 80 per cent of their room temperature
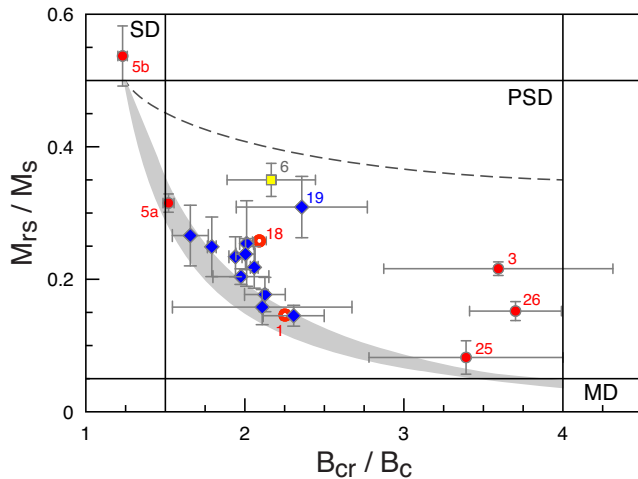
Figure 3. Day plot. Per rock-magnetic group the sites are depicted with a different colour/symbol: group L in yellow squares, M in filled red circles, M* in open red circles, and H in blue diamonds. One standard deviation intervals are shown as black lines. The single (SD), pseudo-single (PSD), and multi-domain (MD) areas are indicated, the grey shading is the area between the theoretically predicted SD+MD mixing lines of the fine and coarse gained end members; the grey dashed line is the SP+SD mixing line (Dunlop 2002). Site numbers are provided for samples discussed in the main text.

susceptibility at 400 °C (Fig. 2d), and generally do not lose more than 20 per cent of their NRM before 300 °C is reached (Fig. 2h). Except for site 19, all group H samples coincide with the SD+MD mixing lines in the Day-plot (Fig. 3) and are characterized as PSD.

4 PALAEOMAGNETIC DIRECTIONS

To obtain the most meaningful palaeodirections, the 'X-samples' were given priority while selecting samples for the demagnetization experiments. For each site at least four samples were thermally demagnetized in 13 steps until <5 per cent of the NRM remained at 600 °C using an ASC-TD48 furnace and a 2G cryogenic magnetometer (Figs 2e–h). Between 80 and 400 °C, steps of 40 °C were used, while above 400 °C, the step size was 50 °C. The magnetic moment of some samples was beyond the dynamic range of the 2G cryogenic magnetometer, so those samples were measured on an AGICO JR-6 Spinner magnetometer. Six samples per site were demagnetized by AF on a robotized 2G cryogenic magnetometer with AF coils attached to the system (Figs 2i–l). Fifteen steps were used: 2.5 mT steps until 10 mT, 5 mT steps until 30 mT and 10 mT steps up to 100 mT. Generally less than 10 per cent of the NRM remained after 100 mT AF demagnetization. The obtained palaeomagnetic directions were averaged, both per site and per age group, with Fisher statistics. Samples that deviated more than 45° from the calculated mean were excluded from the analyses and the mean direction, α_{95}, and precision parameter (k) were recalculated.

The obtained site means have small $\alpha 95$, although k-values for some sites are rather low (between 50 and 100); the direction of site 20 has a k-value of 31.7, therefore its reliability may be doubted (Table 2). The palaeodirections are generally within the expected range of secular variation for this latitude (GAD inclination: ∼58°). The direction of site 26 (declination: 41.6°; inclination: 35.6°; age: 9.7 ka) deviates more from true North than might be expected for 'normal' secular variation and its inclination is rather shallow. This deviation is unexplained; as this site was rather covered by

vegetation we cannot exclude that the sampled blocks of lava may have moved after solidification, although there was no direct evidence of post-cooling movement of the outcrop.

5 PALAEOINTENSITIES

Obtaining reliable estimates of the palaeofield's intensity is notoriously difficult. Here we applied three different techniques to our suite of samples: IZZI-Thellier experiments, the MSP technique, and the calibrated pseudo-Thellier method. The starting conditions of all three protocols were optimized based on the rock-magnetic classification and demagnetization behaviour as previously outlined.

5.1 IZZI-Thellier

The IZZI-Thellier technique (Tauxe & Staudigel 2004) is arguably the most widely used palaeointensity protocol today. It performs particularly well to suppress—or at least identify—multidomain effects that may arise from the multiple heating steps inherent to Thellier-style protocols (Tauxe & Staudigel 2004; Yu & Tauxe 2005; Shaar *et al.* 2011; Paterson *et al.* 2015). In this study IZZI-Thellier experiments were done in two batches: first four to seven samples per site were measured: 86 samples in total. These samples were divided in three groups based on the rock-magnetic analyses and the temperature steps were chosen accordingly; for example smaller temperature steps below 300 °C for L-type samples, and smaller temperature steps above 400 °C for H-type samples. The three series consist of at least 11 temperature steps each; both pTRM-checks (Coe 1967) and pTRM-tail-checks (Riisager & Riisager 2001) were applied every other temperature step. Magnetizations were measured on a 2G cryogenic magnetometer; if the moment of a sample was beyond the dynamic range of this instrument, such samples were measured on an AGICO JR-6 spinner magnetometer. Heating, both in-field and in zero fields, was done in an ASC-48TD thermal demagnetizer. The IZZI-Thellier data were interpreted using the ThellierTool 4.2 software (Leonhardt *et al.* 2004), which implies that some parameters (such as DRAT$_{tail}$) must be derived from the ThellierTool output using the Standard Palaeointensity Definitions (Paterson *et al.* 2014), since they are not provided by the program. To assess the quality of our results we used four sets of criteria: TTA, TTB (Leonhardt *et al.* 2004) and SELCRIT-01 (Selkin & Tauxe 2000) as modified by Paterson *et al.* (2014); and CLASS-A (de Groot *et al.* 2014).

From the 86 samples in this first group only seven samples passed one (or more) of these sets of selection criteria. Most samples failed due to multidomain effects indicated by either excessive 'zigzagging' or 'sagging' in the Arai diagrams (e.g. Figs 4e and f). None of the sites yielded enough acceptable results to produce meaningful site averages and a check for in-site consistency of the obtained palaeointensities. Therefore, we measured a second series of Thellier experiments for which we selected samples from the five most promising sites. For sites 3 (1761 AD) and 18 (283 AD) five samples were selected, and for sites 14 (25.7 ka), and 21 and 24 (both 46.3 ka) an additional six samples were measured. The boundary conditions of the second batch of Thellier experiments were changed following the suggestions of Paterson *et al.* (2015) to suppress multidomain effects. The samples in the first batch of Thellier experiments were placed randomly in the furnace, in the second batch the samples were placed such that the maximum angle between the NRM and the applied field was <90°. Moreover, the DC field was increased
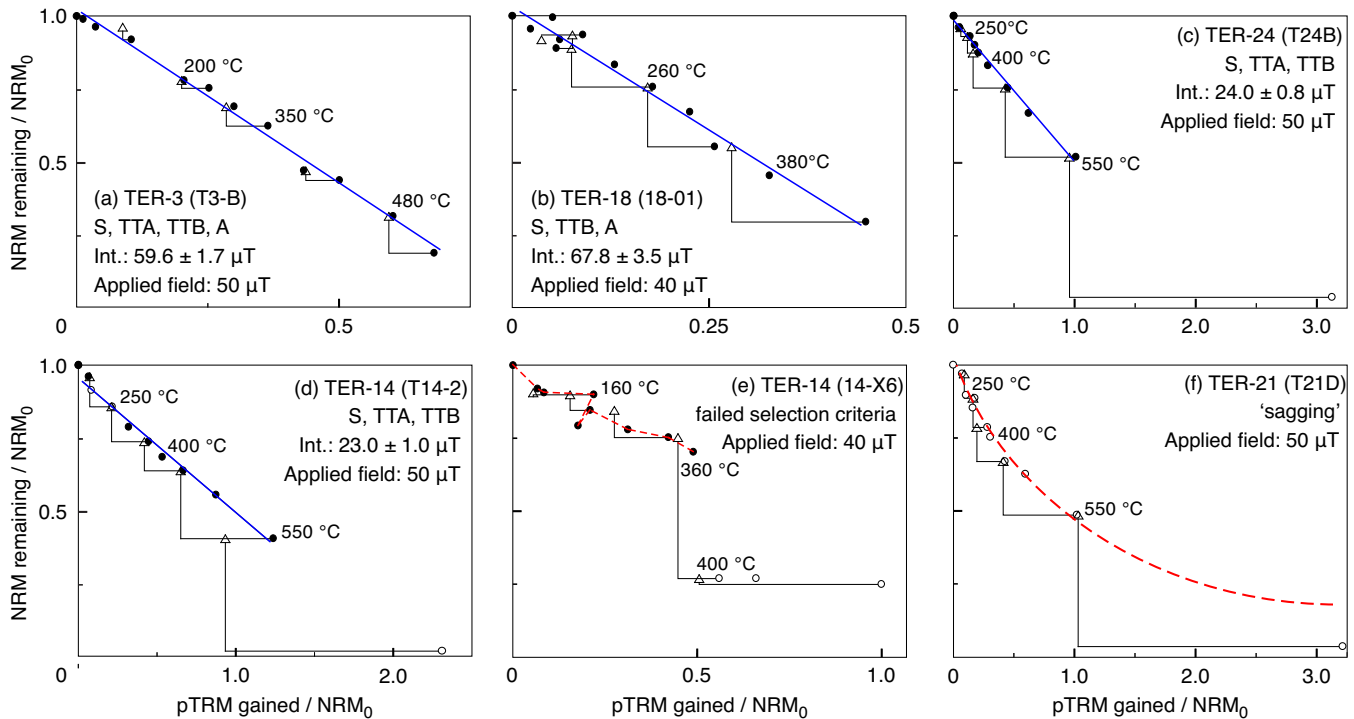
Figure 4. IZZI-Thellier results. Six examples of typical IZZI-Thellier results passing the different sets of selection criteria applied. Data points considered for the linear interpolation (blue line) are closed circles, discarded data points are open circles. Checks are open triangles. Both axes are normalized to the starting NRM (NRM_0). Some characteristic temperatures are indicated, as well as the site and sample code (between brackets) and the obtained palaeointensity (Int.) with its one standard deviation interval. The sets of selection criteria passed are specified in each panel: S, SELCRIT-01 (Selkin & Tauxe 2000); TTA, ThellierTool A (Leonhardt *et al.* 2004); TTB, ThellierTool B (Leonhardt *et al.* 2004); all as modified by (Paterson *et al.* 2014); and A, CLASS-A (de Groot *et al.* 2014). Sample T14-2 (d) and 14-X6 are sister specimens from the same outcrop, the differences in technical quality between the two possibly arise from changes in the boundary conditions between the two experiments in an attempt to suppress MD effects (see main text). Samples 14-X6 (e) and T21D (f) are not interpreted because of failing all sets of selection criteria and prominent sagging, respectively.

from 40 μT in the first batch to 50 μT in the second From the 28 samples in the second set, 21 passed at least one of the sets of selection criteria applied.

Site 21 was the only site that produced technically coherent results but revealed prominent MD behaviour (i.e. sagging) in spite of the efforts to suppress these effects by aligning the samples with the field and increasing the magnitude of the field applied (Fig. 4f). Besides site 21, the IZZI-Thellier results obtained from rock-magnetic group H reveal remarkably stable and linear behaviour up to 550 °C (sites 14 and 24; Figs 4d and c, respectively). The samples from group M* (site 18), presumably with a Hopkinson peak below room temperature, reveal more scatter at lower temperatures, but yield interpretable lines (Fig. 4b). Samples from site 3 (group M) were interpreted over the largest fraction ($f \sim 0.8$ at 520 °C; Fig. 4a) and therefore mostly pass the criteria for CLASS-A, a set that particularly emphasizes the fraction and linearity of the Thellier interpretation (de Groot *et al.* 2014).

Averaging all successful IZZI-Thellier results per age group yielded reliable palaeointensity estimates for sites 3, 14, 18 and 24. All averaged intensities produced are the result of at least five independent samples, and the standard deviation over the mean is <13.4 per cent for all four sites. Assuming normally distributed variation within the sites the 95 per cent confidence intervals are calculated using the Student's *t* distribution given by the standard deviation divided by the square root of the number of samples times the appropriate *t*-value. The two pre-Holocene units yielded (with their 95 per cent confidence intervals) 24.7 ± 2.9 μT (23 718 BC) and 24.3 ± 3.0 μT (44 323 BC), respectively; the two success-

ful Holocene lava flows produced 62.6 ± 2.7 μT (1761 AD), and 64.7 ± 7.3 μT (283 AD; Table 3). All details, obtained parameters, and the selection criteria applied are in Table S1.

5.2 Multispecimen technique

The multiple heating steps in Thellier-style experiments often induce alteration in the majority of samples taken from igneous rocks (e.g. Riisager & Riisager 2001; Valet 2003). To reduce the number of heating steps Dekkers & Böhnel (2006) introduced the MSP palaeointensity technique. Instead of assessing the magnetic behaviour of the samples as function of temperature, the MSP technique considers the change in magnetization as function of the applied field at a constant temperature. Therefore multiple specimens can be used to derive a single palaeointensity estimate. A major drawback of this method is that the samples need to be aligned with their NRM to the field applied in the furnace; (viscous) overprints in the samples may therefore introduce bias in the experiment. Only samples that show no overprints in the thermal demagnetization experiments should be used for MSP-style protocols.

The original MSP technique (further referred to as MSP-DB) did not correct for potential tail and/or domain state effects that might already occur during a single heating step. To this end Fabian & Leonhardt (2010) improved the MSP-DB protocol by adding three extra heating steps to identify and correct for these potential domain state effects, resulting in the MSP-DSC (domain state corrected) method. Furthermore, a check for potential alteration was added

Table 3. Palaeointensity results. The palaeointensity results are grouped by site/age, per result the following is specified: site number, age, palaeointensity method (MSP, multispecimen technique; IZZI, IZZI-Thellier protocol; pTh, pseudo-Thellier technique), the number of specimens on which the mean is based (*n*, number of accepted samples; *N*, number of samples measured; * for the IZZI-Thellier experiments the number of samples in the second batch are specified, the numbers from the first batch are between brackets, see main text), the obtained mean palaeointensity with its associated standard deviation (*SD*; the *SD* of the pseudo-Thellier results is calculated before calibration (see Tables S1 and S2), hence not included in this table), 95 per cent confidence interval (95 per cent CI; the confidence interval for the MSP result is non-Gaussian, hence not specified), the lower and upper bound of the confidence interval, and the standard deviation divided by the palaeointensity (for the pseudo-Thellier results these values are calculated before the conversion to absolute palaeointensities as the constant in the calibration formula would lead to non-Gaussian error distributions, see Tables S1 and S2). Per site the average of the different methods are given (bold), together with their standard deviation are given below the average, and the fraction of the SD over the mean palaeointensity is expressed as a percentage (in bold, between brackets). The pseudo-Thellier results of sites 3, 5 and 6 were published before in Pimentel *et al.* (2016).

Site(s)	Age	Method	*n/N*	Palaeoint. (μT)	SD (μT)	95% CI (μT)	Lower bound (μT)	Upper bound (μT)	SD/palaeoint. (−) ∼2.4%
3	1761 AD	MSP	10/10	53.3	–	–	52.1	54.7	∼2.4%
3	1761 AD	IZZI	5/5 (0/7)*	62.6	2.2	2.7	59.9	65.3	3.5%
3, 5, 6	1761 AD	pTh	12/18	58.7	–	5.4	53.3	64.1	19.3%
				58.2					
				4.7 (8.0%)					
18	283 AD	IZZI	5/6 (3/4)*	64.7	8.7	7.3	57.4	72.0	13.4%
18, 19	283 AD	pTh	7/12	66.4	–	4.6	61.8	70.9	9.6%
				65.6					
				1.2 (1.8%)					
7, 8	3210 BC	pTh	13/18	36.1	–	2.1	34.0	38.2	16.1%
26	7673 BC	pTh	5/6	34.7	–	3.5	31.2	38.1	13.8%
14	23718 BC	IZZI	6/6 (0/7)*	24.7	2.7	2.9	21.8	27.6	11.0%
14	23718 BC	pTh	6/6	24.1	–	0.8	23.2	24.9	8.5%
				24.4					
				0.4 (1.7%)					
24	44323 BC	IZZI	6/6 (−)*	24.3	2.9	3.0	21.3	27.3	11.9%
16, 21, 24	44323 BC	pTh	12/18	23.8	–	0.8	22.9	24.6	14.4%
				24.1					
				0.4 (1.5%)					

to the technique: at sample level the change between a repeated heating step and the first heating step can be assessed, much akin to a pTRM-check in the IZZI-Thellier protocol. In the MSP-DSC protocol this alteration is described by the ε_{alt} parameter (Fabian & Leonhardt 2010). The domain state proxy, the 'α-parameter', was set to 0.5 as suggested by Fabian & Leonhardt (2010).

Up to three potential temperatures for MSP experiments were selected for the sites that did not show overprints during the de-magnetization experiments. Ideally, samples unblock at least 15 per cent of their NRM at the selected temperature and are below their alteration temperature as derived from the χ–T analyses (Table 2). These potential MSP temperatures were tested with a single-core ARM-test to detect subtle magnetic alteration (i.e. trans-domain changes) that are not revealed by the χ–T analyses at those specific temperatures (de Groot *et al.* 2012). Out of the 30 ARM-tests done, nine were successful; MSP-DSC experiments were carried out for these nine combinations of site and temperature. The MSP results were interpreted using MSP-Tool (Monster *et al.* 2015). To deem the outcome of a MSP-DSC experiment reliable, the alteration induced during the experiment should be minimal: we therefore reject samples with $|\varepsilon_{alt}| > 5$ per cent; and only accept sites that produce an average ε_{alt} for all samples included in the interpretation between −3 and 3 per cent. Furthermore, the linear fit through the data should intercept the *y*-axis close to the theoretically predicted −1; MSP-DSC interpretations that intersect the *y*-axis above −0.9 or below −1.1 are rejected.

Scrutinizing our data with these criteria yields one reliable MSP-DSC outcome: site 3 (1761 AD) produces a palaeointensity of 53.3 μT, with a 95 per cent bootstrapped confidence interval from 52.1 to 54.7 μT (Fig. 5). This experiment was done at 300 °C; the associated average ε_{alt} of 1.6 per cent, and the *x*-axis intercept of −0.96 are both well within the criteria outlined above.

5.3 Calibrated pseudo-Thellier experiments

The calibrated pseudo-Thellier technique (de Groot *et al.* 2013) avoids thermally induced alteration that may occur in conventional palaeointensity methods. This relatively new method converts the outcome of relative pseudo-Thellier experiments (Tauxe *et al.* 1995) on lavas into absolute estimates of the Earth's palaeofield. The pseudo-Thellier technique is much akin to other Thellier-style experiments, but applies alternating fields to impart magnetizations in the sample [i.e. (p)ARMs] instead of using thermal steps [i.e. (p)TRMs]. When applied to lavas, the behaviour of the pseudo-Thellier technique depends on both the chemical composition of the remanence carrying grains (de Groot *et al.* 2015) and their grain size distribution (Yu *et al.* 2003). For these parameters there are selection criteria that should be met, before the pseudo-Thellier results can be reliably and faithfully converted into absolute estimates of the palaeofield's intensity. Samples that are associated with high titanium content in the remanence carrying grains and associated low Curie temperatures cannot be reliably used for the calibrated pseudo-Thellier technique. This is quantified by excluding de Groot *et al.*'s (2015) rock-magnetic group *L** —samples that lose more than 80 per cent of their room temperature susceptibility
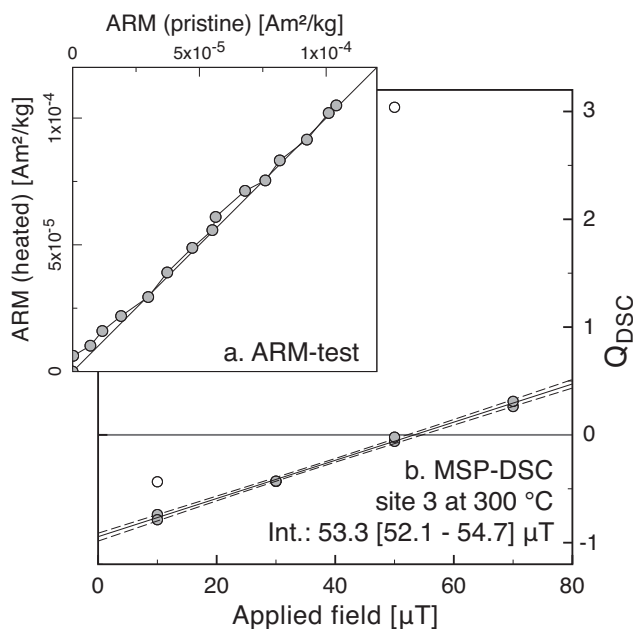
Figure 5. Multispecimen result. The ARM-test for site 3 shows no change in the behaviour of an ARM acquisition after heating samples to 300 °C (a). The results of the pristine samples are on the horizontal axis; the measurements after heating are on the vertical axis. The MSP-DSC experiment (b) reveals little scatter (interpreted data are grey circles), after two outliers are identified and removed (open circles). The *y*-axis is cut-off near the theoretically predicted-1, and alteration during the experiment was minimal (see main text). The obtained palaeointensity (53.3 μT) is specified together with its one standard deviation interval.

before reaching 150 °C and exhibit a decrease in susceptibility when heated from room temperature onwards (i.e. implying a Hopkinson peak below room temperature)—from the pseudo-Thellier interpretation. None of the sites in this study is characterized as such. The grain size selection is done at specimen level using a parameter that can be derived from the pseudo-Thellier experiments: $B_{\frac{1}{2}\text{ARM}}$, half the value of the field that imparts the saturated ARM, in our experiments at 300 mT. Samples with a $B_{\frac{1}{2}\text{ARM}}$ between 23 and 63 mT can be reliably converted into absolute palaeointensities by a linear calibration relation (de Groot *et al.* 2013).

The first step in the pseudo-Thellier experiment is to AF demagnetize the samples in 18 steps up to 300 mT (2.5 mT steps until 10 mT, 5 mT steps until 30 mT, 10 mT steps until 100 mT, and 150 and 300 mT). For the steps up to 100 mT measuring and demagnetization was done on a robotized 2G cryogenic magnetometer with AF coils attached to the system; higher fields were applied by a laboratory-built AF coil and magnetizations measured on the same robotized magnetometer. The second step of the pseudo-Thellier method consists of an ARM-acquisition using the same fields as applied during the AF demagnetization with a dc field of 40 μT; fields up to 150 mT were magnetized and measured on the robotized system, only the 300 mT step was imparted using the manual AF coil. The last step is to AF demagnetize the acquired ARM in the samples, again using the same fields; the fields up to 100 mT were measured on the robotized system, higher fields were not measured. To obtain a reliable pseudo-Thellier result the ARMs should be carried by the same grains that stored the NRM in the samples. This is checked by comparing the AF demagnetization spectra of the NRM (step 1) and the acquired ARM (step 3): if the same grains store the NRM and ARM the demagnetization spectra should be linear when plotted against each other. For these particular AF fields the pseudo-Thellier slope in the Arai plot (NRM remaining versus ARM acquired) are interpreted.

Per site, six samples were subjected to the routine outlined above, 114 samples were processed in total. Of those, 17 were not interpretable—that is non-linear behaviour in either the ARM-NRM demagnetization spectra or pseudo-Thellier Arai diagrams. Out of the 97 interpretable samples, 65 have a $B_{\frac{1}{2}\text{ARM}}$ between 23 and 63 mT and therefore pass the grain size selection criterion. All samples are then grouped by their age, in nine age groups (that may consist of samples from more than one site). If three or more successful pseudo-Thellier results are available they can be averaged into a mean pseudo-Thellier slope and its associated standard deviation and 95 per cent confidence interval can be determined (Table 4). The 95 per cent confidence intervals were calculated using the same statistical method as used for the IZZI Thellier results: the student's t-distribution. For one site the standard deviation is more than 20 per cent of the obtained pseudo-Thellier average, this result was therefore rejected. The remaining eight pseudo-Thellier averages can be converted into absolute estimates of the palaeofield. The pseudo-Thellier results at specimen level are in Table S2.

Table 4. Pseudo-Thellier results. Per age group the following are specified: age, the number of interpretable samples that pass the selection criterion (*n*) and the number of measured (*N*) samples, the average absolute pseudo-Thellier slope (pTh slope), the standard deviation of the accepted pseudo-Thellier results (*SD*), the fraction of the standard deviation over the obtained intensity (>20 per cent is rejected, *SD*/mean), the 95 per cent confidence interval (95 per cent CI), the absolute intensity obtained using the original calibration formula [Cal. Int. (2013)], with its 95 per cent confidence interval [95 per cent CI (2013)], the absolute intensity obtained using the formula presented in this study: $B = 7.718 \times |\text{pTh slope}| + 14.600$ (Cal. Int. [μT] (this study)), with its 95 per cent confidence interval [95 per cent CI (this study)], the absolute difference between palaeointensities obtained with the two calibration formulae (ΔInt. [μT]), and this difference expressed as a fraction of the original (2013) calibration formula (ΔInt. [per cent]). Rejected or unsuccessful sites are in italics.

Age group	*n/N*	pTh slope	*SD*	*SD*/mean	95% CI	Cal. Int. (2013) (μT)	95% CI (2013) (μT)	Cal. Int. (this study) (μT)	95% CI (this study) (μT)	ΔInt. (μT)	ΔInt. (%)
1761 AD	12/18	5.71	1.11	19.3%	0.70	56.7	5.2	58.7	5.4	1.9	3.3
94 AD	*4/12*	*6.49*	*2.21*	*34.0%*	*3.51*	*62.5*	*25.9*	*64.7*	*27.1*	*2.2*	*3.4%*
283 AD	7/12	6.71	0.64	9.6%	0.59	64.1	4.3	66.4	4.6	2.3	3.4%
3210 BC	13/18	2.79	0.45	16.1%	0.27	35.2	2.0	36.1	2.1	0.9	2.5%
7673 BC	5/6	2.60	0.36	13.8%	0.45	33.8	3.3	34.7	3.5	0.8	2.4%
9719 BC	*2/6*										
23718 BC	6/6	1.23	0.10	8.5%	0.11	23.7	0.8	24.1	0.8	0.4	1.5%
44323 BC	12/18	1.19	0.17	14.4%	0.11	23.4	0.8	23.8	0.8	0.4	1.5%
116 ka	*2/6*										
401 ka	*1/6*										

Figure 6. Updating the pseudo-Thellier calibration. All pseudo-Thellier results produced for Hawaii (de Groot *et al.* 2013), the Canary Islands (de Groot *et al.* 2015), and this study are plotted against their corresponding IGRF/GUFM1 (Jackson *et al.* 2000; yellow triangles), IZZI-Thellier (green squares), microwave-Thellier (purple diamonds), and MSP-DSC (red circles) values. The data error bars for data from the present study are in black; the literature data has grey error bars. With the new low palaeointensity data we can now improve the calibration relation and update it to: $B_{abs} = 7.718 \times |$pseudo-Thellier slope$| + 14.600$ (blue line and shaded 95 per cent confidence interval). Previous calibration relations are dashed red lines.

The first pseudo-Thellier calibration relation was put forward by de Groot *et al.* (2013), and was based on historic samples (1840–2010 AD) from Hawai'i for which the intensity of the field at the time of cooling is known. This resulted in a calibration relation that is independent of other palaeointensity techniques, but is defined on a rather narrow range of intensities; i.e. the pseudo-Thellier behaviour was extrapolated below ~34 µT and above 40 µT. To extend this range the calibration relation was updated by including sites from the Canary Islands for which thermal and microwave palaeointensity methods were successful (de Groot *et al.* 2015). This added sites with palaeointensities up to 80 µT to the calibration relation, and showed that the calibration relation is linear between 34 and 80 µT at least; furthermore, it was possible to provide a meaningful confidence interval around the linear relation. The behaviour for lower fields and the issue of the non-zero *y*-axis intercept of the calibration relation (de Groot *et al.* 2013, 2015) were not solved. An inevitable draw-back of using data from other palaeointensity methods, however, is that the calibrated pseudo-Thellier results become dependent on the other methods, that is a systematic bias in (one of the) other methods propagates into the absolute palaeointensity estimates produced by the pseudo-Thellier conversion. Here we present both IZZI-Thellier and pseudo-Thellier results for cooling units from periods of known low intensities and report estimates as low as 24 µT. We therefore enlarge the range of intensities on which the calibration relation is based and use these data to update the calibration relation proposed by de Groot *et al.* (2015) to $B_{abs} = 7.718 \times |$pseudo-Thellier slope$| + 14.600$ (Fig. 6), and provide the associated 95 per cent confidence interval (Fig. 6).

The eight reliable pseudo-Thellier results are converted into absolute estimates of the palaeofield's intensity using both this new calibration relation and the original calibration relation that is independent of other palaeointensity methods (Table 4). With the new calibration relation an absolute intensity estimate (with its 95 per cent confidence interval) of 58.7 ± 5.4 µT is obtained for the 1761 AD units (sites 3, 5 and 6), with the original relation this site yields 56.7 ± 5.2 µT. The intensity for the 283 AD unit (sites 18 and 19) is also quite high: 66.4 ± 4.6 µT (64.1 ± 4.3 µT with the original

calibration relation). The two older Holocene units (sites 7 & 8 and 26) that were successful yielded lower palaeointensities: 36.1 ± 2.1 and 34.7 ± 3.5 µT for 3210 and 7673 BC, respectively (35.2 ± 2.0 and 33.8 ± 3.3 µT with the original calibration, respectively). The two units with ages close to known excursions of the field (sites 14 and 16, 21 & 24) produce the lowest palaeointensities: 24.1 ± 0.8 and 23.8 ± 0.8 µT, respectively (23.7 ± 0.8 and 23.4 ± 0.8 µT with the original calibration, respectively). The differences between the palaeointensities obtained using the original calibration relation (de Groot *et al.* 2013) are small: the largest deviations occur for higher fields and are ≤2.3 µT, or ≤3.4 per cent.

6 DISCUSSION

6.1 Palaeodirections

The palaeodirections are obtained from samples that are well distributed over the outcrops. Except for sites 11 (401 ka), 14 (25.7 ka) and 20 (9719 BC), the other units are sampled at two or more locations, sometimes kilometres apart; this increases the robustness of the obtained directions. Furthermore, this explains why the *k*-values associated with the directions may be rather low for volcanic products: by sampling the cooling unit over large distances, small post-cooling movements within the outcrop or of the underlying terrain are averaged, lowering the *k*-values, but increasing the reliability of the directions. Moreover, potential local anomalies in the field (Baag *et al.* 1995; Valet & Soler 1999) are suppressed by this sampling strategy.

The declinations (Fig. 7a) and inclinations (Fig. 7b) were compared to the data produced by Di Chiara *et al.* (2012) and the newest generation of geomagnetic field model predictions (Nilsson *et al.* 2014; Pavón-Carrasco *et al.* 2014). Except for site 26 (7673 BC), our data concur well with both data from the nearby island of São Miguel (Di Chiara *et al.* 2012) and the field models. The mean declination of the 1761 AD samples is 22.4° West, and deviates substantially from true North, but this is in close agreement with
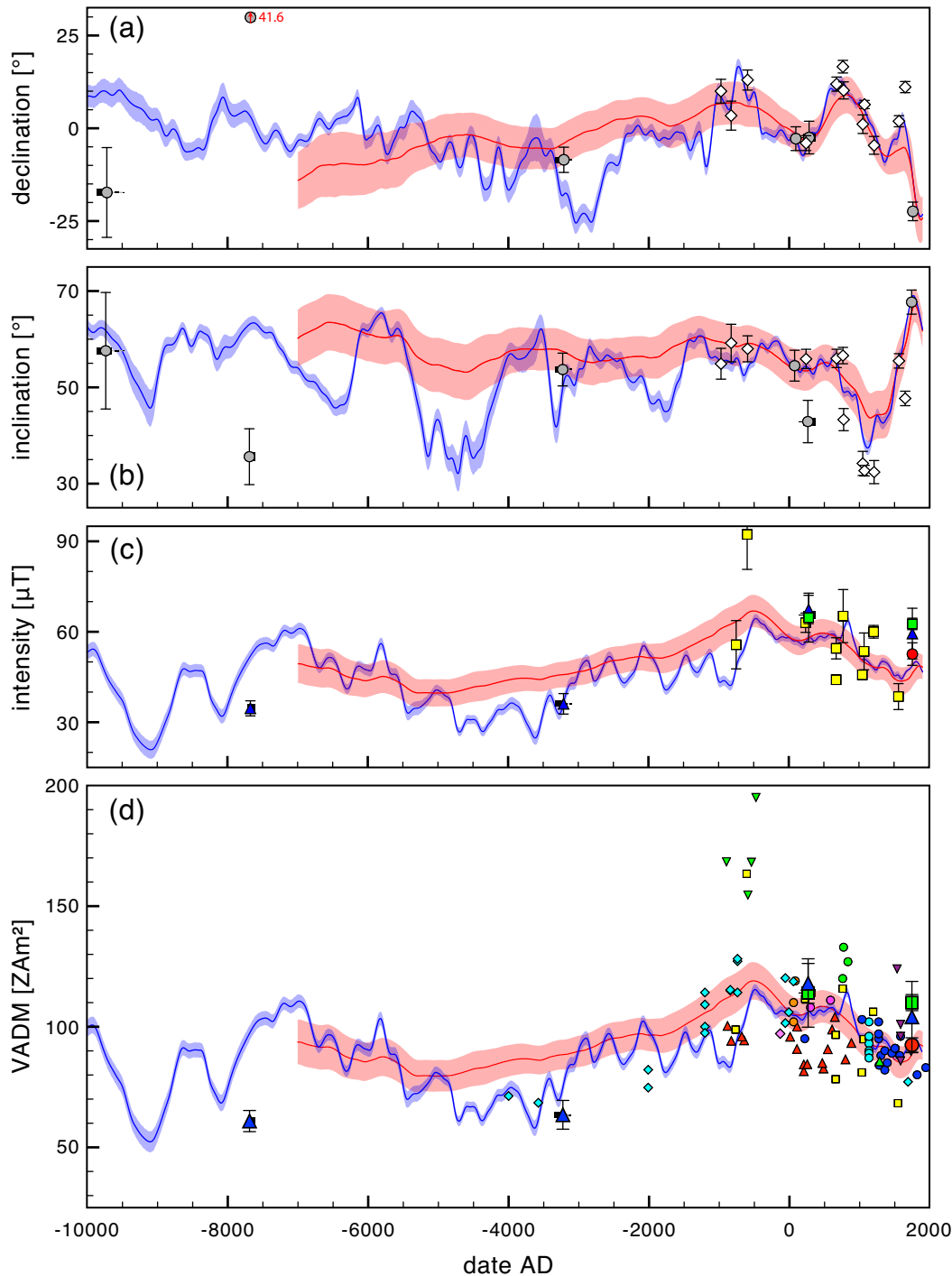
Figure 7. Full vector geomagnetic field record for the Holocene. The declination (a), inclination (b) and intensity (c) results are superimposed on the PFM9K.1b (red line), and SHA.DIF.14k (blue line) geomagnetic field models, with their one standard deviation envelopes (colour shading). The declination and inclination data from this study are depicted as grey circles, with the vertical error bar being the α_{95} interval; data of (Di Chiara *et al.* 2012) are open diamonds. Intensities (c) obtained using the IZZI-Thellier protocol are green squares; the MSP-DSC result is a red circle; blue triangles are the pseudo-Thellier results; data from (Di Chiara *et al.* 2014) are yellow squares. The vertical error bars are the associated confidence intervals in intensity. The horizontal error bars are one-standard-deviation probability intervals of the INTCAL.13 calibration; in some cases the confidence intervals are very small and the error bars are not larger than the data points. If more than one interval was obtained, a horizontal thin grey line connects them and the thickness of the bars is equivalent to their relative probability. The VADM literature data (d) from São Miguel are yellow squares (Di Chiara *et al.* 2014); the Canary Islands are diamonds in blue (de Groot *et al.* 2015) and pink (Ferk *et al.* 2011); West-Africa are triangles (pointing up) in red (Mitra *et al.* (2013) and green (Gómez-Paccard *et al.* 2012b); Portugal are triangles (pointing down) in purple (Hartmann *et al.* 2009) and green (Nachasova & Burakov 2009); Spain are circles in pink (Catanzariti *et al.* 2012), light-blue (Gómez-Paccard *et al.* 2006), dark blue (Gómez-Paccard *et al.* 2008), green (Gómez-Paccard *et al.* 2012a) and orange (Gómez-Paccard *et al.* 2013). Symbols for the data obtained in this study are slightly larger, have error bars, and use the same symbols as in (c).

the geomagnetic model predictions for this age. As mentioned before, the deviation with respect to the GAD prediction of site 26 (declination: 41.6°; inclination: 35.6°; age: 9.7 ka) cannot be explained other than by post-cooling movements although there was no visual evidence that this actually occurred.

6.2 IZZI-Thellier experiments

For our 10 potential ages, reliable IZZI-Thellier results were obtained for four of them, an unusually high success rate for volcanic products (40 per cent); the success rate at sample level, however, is much lower: only 28 of 114 (25 per cent) measured samples passed one or more sets of selection criteria. The adjustments to the Thellier protocol in the second batch of Thellier experiments, following the suggestions of Paterson *et al.* (2015) (reducing the maximum angle between the NRM and the applied field in the furnace to <90° and increasing the applied field to 50 μT), had a positive influence on the technical quality of the results. The Thellier results of sister specimens from site 14, in the second batch, easily passed the sets of selection criteria applied, while samples processed in the first batch did not [compare Fig. 4d (second batch) and 4e (first batch, 'zigzagging')]. The theoretical predictions of increased success rate and suppression of MD effects such as sagging by Paterson *et al.* (2015) are therefore clearly reflected in our experiments. Furthermore it is important to note that there is no correlation between the type of volcanic product and the success rates in IZZI Thellier palaeointensity experiments: both trachytic (sites 3 and 18) and basaltic (sites 14 and 24) lavas, and a welded trachytic ignimbrite (site 14) yielded reliable palaeointensities.

6.3 Calibrated pseudo-Thellier technique

The pseudo-Thellier method yielded reliable estimates for six of the 10 age groups in this study, a success rate of 60 per cent that concurs well with the pseudo-Thellier success rates of 58 and 67 per cent for the Canary Islands (de Groot *et al.* 2015) and Hawaii (de Groot *et al.* 2013), respectively. For four units/ages both the IZZI-Thellier and pseudo-Thellier techniques were successful. These IZZI-Thellier results were used to recalibrate the pseudo-Thellier formula, absolute intensities obtained with this new formula are therefore not independent from the other palaeointensity methods: a bias in the results of the other methods propagates into the calibration relation and therefore into the obtained absolute pseudo-Thellier intensities. Using the data from three independent palaeointensity methods (IZZI-Thellier, Microwave-Thellier (de Groot *et al.* 2015), and MSP) and three different volcanic regions, however, reduces the chances of systematically propagating a bias into the calibration relation. Adding palaeointensity data from other methods validates the calibration relation for a much larger range of intensities (now between 20 and 80 μT) and provides a meaningful confidence interval around the calibration relation (Fig. 6). Moreover, the updated calibration relation yields only very minor changes in absolute palaeointensity estimates with respect to the original calibration relation (de Groot *et al.* 2015; Table 4); for intensities below 100 μT differences are <4 per cent. This elucidates the robustness of the calibration relation obtained here: the relation is (1) insensitive to the addition of new data, (2) based on data from three different volcanic regions (Hawaii, Canary Islands, and Azores), (3) calibrated based on data obtained with three independent palaeointensity techniques and direct field observations, (4) straddles the intensity range from ∼20 to 80 μT and (5) provided together with a confidence in-

terval. We therefore prefer the absolute palaeointensity data that are obtained using the newly proposed calibration relation over the data obtained using the original formula. Nevertheless, the updated calibration relation still misses the origin and its reliability below ∼20 μT cannot be established from the data presented here.

6.4 Multispecimen method

The MSP technique only yielded one reliable estimate of the palaeofield for our 10 possible ages, a success rate of 10 per cent. The MSP result obtained for site 3 is notably lower than the IZZI- and pseudo-Thellier results for the same age: 53.3 μT, versus 62.6 and 58.7 μT, respectively. This trend is also observed when comparing coeval MSP and IZZI- and pseudo-Thellier results produced for the Canary Islands (de Groot *et al.* 2015) and Hawaii (de Groot *et al.* 2013). This may be related to the observation of Cromwell *et al.* (2015) where Thellier-style palaeointensities derived from Kilauea's basaltic lavas tend to produce overestimates of the field. Unfortunately, there are too few coeval MSP and IZZI- and pseudo-Thellier results in the current data sets to perform meaningful statistical analyses and quantify the tentative trend observed.

6.5 The Holocene geomagnetic intensity record for the Azores

We now compare our palaeointensity results from Terceira to the results of the nearby island of São Miguel (Di Chiara *et al.* 2014) and geomagnetic field models (Fig. 7c). One of our palaeointensity estimates (283 AD, derived from sites 18 and 19) is nearly coeval with one of the sites of Di Chiara *et al.* (2014) and their palaeointensities are indistinguishable within error. For a better regional understanding of the Earth's magnetic field, we selected palaeointensity data from a 2500 km radius around the Azores. This circle comprises the Iberia Peninsula, the Canary Islands, parts of North Africa and a very small portion of Southwest England. We considered literature palaeointensity data from these regions that is the mean of at least three independent (mostly Thellier) measurements. Data that originates from Spain (Catanzariti *et al.* 2012; Gómez-Paccard *et al.* 2012, 2013a, 2006, 2008), Portugal (Hartmann *et al.* 2009; Nachasova & Burakov 2009), the Canary Islands (Ferk *et al.* 2011; de Groot *et al.* 2015) and West-Africa (Gómez-Paccard *et al.* 2012b; Mitra *et al.* 2013) fulfil this criterion (Fig. 7d). Most of these data are derived from archaeological artefacts; only the Canary Islands data were obtained from volcanic products. For the last 2000 yr, data are relatively abundant; hence the geomagnetic models fit the data reasonably well, although the extremes that seem to occur in the data (e.g. the high around ∼800 AD and the low ∼400 AD) are inevitably smoothed. Prior to 0 AD the data are scarce and the models deviate substantially from the available data; especially before 1500 BC the models produce rather high VADMs in contrast to the data.

6.6 Brunhes directions and intensities

The pre-Holocene palaeodirections and palaeointensities obtained in our study can be compared to a sediment record from the Azores (Kruiver *et al.* 1999) and the global PISO-1500 stack (Channell & Xuan 2009). The SU92-18 core was taken approximately ∼100 km south of Terceira (37.8°N, 27.2°W) and it comprises the last 276 kyr (Kruiver *et al.* 1999). It was subjected to both directional and pseudo-Thellier (on sediments, hence relative) analyses. The
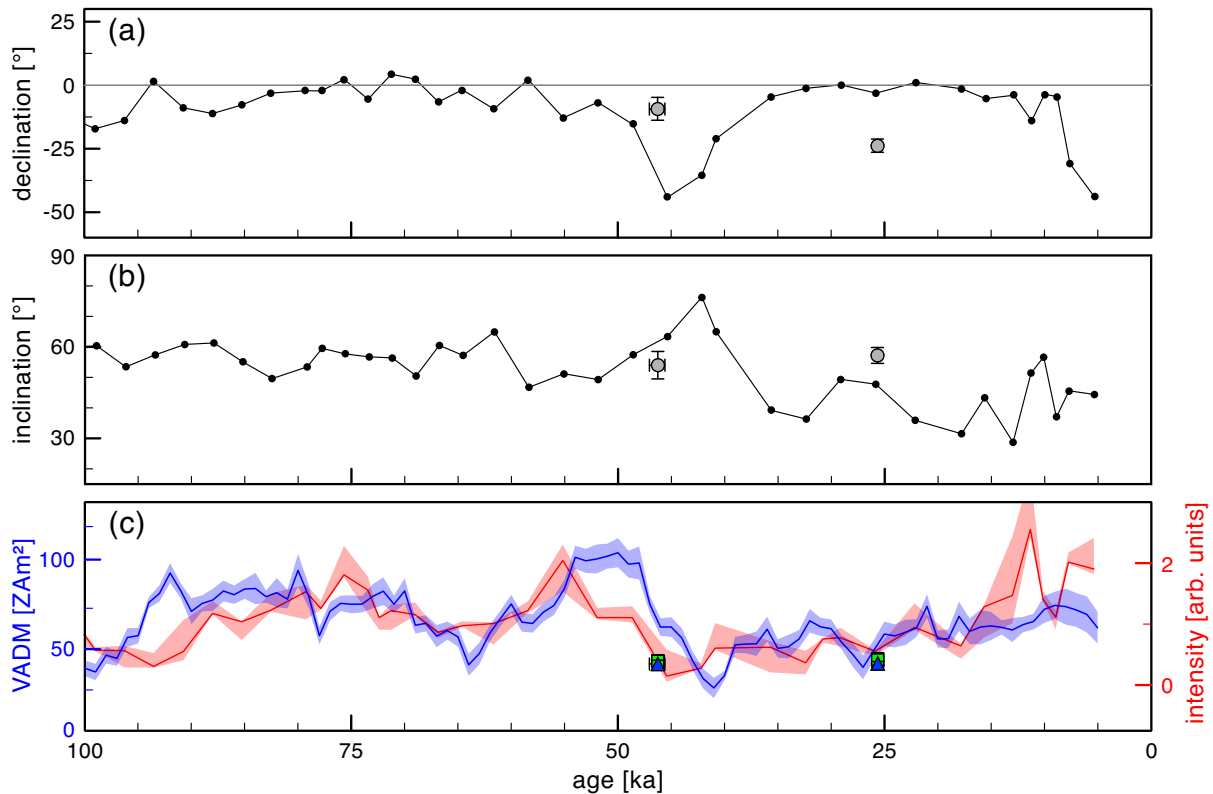
Figure 8. Full-vector geomagnetic record of the Brunhes. The declination (a) and inclination (b) obtained for 25.7 and 46.3 ka are superimposed on the directional records obtain from core SU92-18 (Kruiver *et al.* 1999). The declinations and inclinations of our sites deviate substantially from the marine record; this may be attributed to secular variation being smoothed in the sediments. Our intensity data coincides with the lows in the relative pseudo-Thellier record derived from the SU92-18 core (Kruiver *et al.* 1999; red line and shading in c), although the low intensity at 46.3 ka predates the low intensities in the PISO-1500 stack (Channell & Xuan 2009; blue line and shading in c) by ~5 kyr.

core was taken unoriented, so the mean declination was put to true North. The data of our sites 14 (25.7 ka) and 16, 21 and 24 (46.3 ka) can be compared to this record (Figs 8a and b). However, it must be emphasized that our cooling units take spot readings of the field while the sediments inherently smooth the behaviour of the geomagnetic field in time.

Between ~35 and ~48 ka the declination in the sediments deviates up to 45° from true North; in the same time interval the inclination peaks at >75°, this is attributed to the Laschamps geomagnetic excursion (Kruiver *et al.* 1999). Our directions at 46.3 ka are much closer to the expected direction from a GAD, but the intensity (VADM) is as low as 42 ZAm² and coincides with the lowest relative palaeointensity values that occur in the relative pseudo-Thellier curve (Kruiver *et al.* 1999; Fig. 8c). The PISO-1500 stack has its lowest intensity values ~5 kyr later, that is at ~41 ka (Channell & Xuan 2009). This implies that the excursional behaviour of the geomagnetic field occurred earlier in the Azores region and over a longer time span than the duration of the Laschamps excursion in PISO-1500 stack.

At 25.7 ka we report low palaeointensities: a VADM of 43 ZAm² (Fig. 8c). This concurs with the low intensities in the PISO-1500 stack at ~26.5 ka, that may be attributed to the Mono Lake excursion, although the exact timing of that geomagnetic phenomenon is still under debate (e.g. Cox *et al.* 2012; Vazquez & Lidzbarski 2012). Our declination for this site deviates considerably from true North (23.8°W), but this is well within the 'normal' range of secular variation for this latitude as the 1761 AD-sites yielded a declination of 22.4°W.

7 CONCLUSIONS

We obtained robust estimates of the palaeofield's intensity for six out of 10 sampled cooling units from the island of Terceira, Azores. This unusually high success rate is attributed to (1) sampling units at several locations and (2) adopting a multimethod palaeointensity approach. Adding data from samples that cooled in a relatively weak Earth's magnetic field further refined the pseudo-Thellier calibration relation. Although this makes the pseudo-Thellier results dependent on the other palaeointensity methods, the robustness of the calibration relation is increased as it is now based upon data ranging from ~20 to ~80 μT and from three different volcanic edifices (Hawai'i, the Canary Islands, and Terceira). Moreover, the changes between the original (de Groot *et al.* 2013) and the currently proposed relation are less than 4 per cent for fields <100 μT. The palaeodirections and palaeointensities presented here increase the accuracy and resolution of the Holocene secular variation curve for the Azores region. Moreover, tentative constraints on the regional behaviour at the time of the Laschamps excursion are provided: the geomagnetic field is quite weak (~42 ZAm²) up to 5 kyr before the Laschamps excursion occurs in the PISO-1500 stack.

REFERENCES

Baag, C., Helsley, C.E., Xu, S. & Lienert, B.R., 1995. Deflection of paleomagnetic directions due to magnetization of the underlying terrain, *J. geophys. Res.,* **100,** 10 013–10 027.

Calvert, A.T., Moore, R.B., McGeehin, J.P. & Rodrigues da Silva, A.M., 2006. Volcanic history and ^{40}Ar/^{39}Ar and ^{14}C geochronology of Terceira Island, Azores, Portugal, *J. Volc. Geotherm. Res.,* **156,** 103–115.

Catanzariti, G., Gómez-Paccard, M., McIntosh, G., Pavón-Carrasco, F.J., Chauvin, A. & Osete, M.L., 2012. New archaeomagnetic data recovered from the study of Roman and Visigothic remains from central Spain (3rd-7th centuries), *Geophys. J. Int.,* **188,** 979–993.

Channell, J. & Xuan, C., 2009. Stacking paleointensity and oxygen isotope data for the last 1.5 Myr (PISO-1500), *Earth planet. Sci. Lett.,* **283**(1–4), 14–23.

Coe, R.S., 1967. Paleo-intensities of the Earth's magnetic field determined from Tertiary and Quaternary rocks, *J. geophys. Res.,* **72,** 3247–3262.

Cox, S.E., Farley, K.A. & Hemming, S.R., 2012. Insights into the age of the Mono Lake excursion and magmatic crystal residence time from (U-Th)/He and ^{230}Th dating of volcanic allanite, *Earth planet. Sci. Lett.,* **319–320,** 178–184.

Cromwell, G., Tauxe, L., Staudigel, H. & Ron, H., 2015. Paleointensity estimates from historic and modern Hawaiian lava flows using glassy basalt as a primary source material, *Phys. Earth planet. Inter.,* **241,** 44–56.

Day, R., Fuller, M. & Schmidt, V., 1977. Hysteresis properties of titanomagnetites: grain-size and compositional dependence, *Phys. Earth planet. Inter.,* **13,** 260–267.

de Groot, L.V., Dekkers, M.J. & Mullender, T., 2012. Exploring the potential of acquisition curves of the anhysteretic remanent magnetization as a tool to detect subtle magnetic alteration induced by heating, *Phys. Earth planet. Inter.,* **194–195,** 71–84.

de Groot, L.V., Biggin, A.J. & Dekkers, M.J., 2013. Rapid regional perturbations to the recent global geomagnetic decay revealed by a new Hawaiian record, *Nat Commun.,* **4,** doi:10.1038/ncomms3727.

de Groot, L.V., Dekkers, M.J., Visscher, M. & ter Maat, G.W., 2014. Magnetic properties and paleointensities as function of depth in a Hawaiian lava flow, *Geochem. Geophys. Geosyst.,* **15,** 1096–1112.

de Groot, L.V. *et al.*, 2015. High paleointensities for the Canary Islands constrain the Levant geomagnetic high, *Earth planet. Sci. Lett.,* **419,** 154–167.

Dekkers, M.J. & Böhnel, H.N., 2006. Reliable absolute palaeointensities independent of magnetic domain state, *Earth planet. Sci. Lett.,* **248,** 508–517.

Di Chiara, A., Speranza, F. & Porreca, M., 2012. Paleomagnetic secular variation at the Azores during the last 3 ka, *J. geophys. Res.,* **117,** B07101, doi:10.1029/2012JB009285.

Di Chiara, A., Tauxe, L. & Speranza, F., 2014. Paleointensity determination from São Miguel (Azores Archipelago) over the last 3 ka, *Phys. Earth planet. Inter.,* **234,** 1–13.

Dunlop, D.J., 2002. Theory and application of the Day plot (Mrs/Ms versus Hcr/Hc): 1. Theoretical curves and tests using titanomagnetite data, *J. geophys. Res.,* **107,** 2056, doi:10.1029/2001JB000486.

Fabian, K. & Leonhardt, R., 2010. Multiple-specimen absolute paleointensity determination: an optimal protocol including pTRM normalization, domain-state correction, and alteration test, *Earth planet. Sci. Lett.,* **297,** 84–94.

Ferk, A., Leonhardt, R., von Aulock, F.W., Hess, K.U. & Dingwell, D.B., 2011. Paleointensities of phonolitic obsidian: influence of emplacement rotations and devitrification, *J. geophys. Res.,* **116,** B12113, doi:10.1029/2011JB008397

Gertisser, R. *et al.,* 2010. Ignimbrite stratigraphy and chronology on Terceira Island, *Azores, Geol. Soc. Am. Spec. Papers,* **464,** 133–154.

Gómez-Paccard, M., Chauvin, A., Lanos, P., Thiriot, J. & Jiménez-Castillo, P., 2006. Archeomagnetic study of seven contemporaneous kilns from Murcia (Spain), *Phys. Earth planet. Inter.,* **157,** 16–32.

Gómez-Paccard, M., Chauvin, A., Lanos, P. & Thiriot, J., 2008. New archeointensity data from Spain and the geomagnetic dipole moment in western Europe over the past 2000 years, *J. geophys. Res.,* **113,** B09103, doi:10.1029/2008JB005582.

Gómez-Paccard, M. *et al.,* 2012a. Improving our knowledge of rapid geomagnetic field intensity changes observed in Europe between 200 and 1400 AD, *Earth planet. Sci. Lett.,* **355–356,** 131–143.

Gómez-Paccard, M., McIntosh, G., Chauvin, A., Beamud, E., Pavón-Carrasco, F.J. & Thiriot, J., 2012b. Archaeomagnetic and rock magnetic study of six kilns from North Africa (Tunisia and Morocco), *Geophys. J. Int.,* **189,** 169–186.

Gómez-Paccard, M., Beamud, E., McIntosh, G. & Larrasoana, J.C., 2013. New archaeomagnetic data recovered from the study of three Roman kilns from North-East Spain: a contribution to the Iberian palaeosecular variation curve, *Archaeometry,* **55,** 159–177.

Hartmann, G.A., Trindade, R.I., Goguitchaichvili, A., Etchevarne, C., Morales, J. & Afonso, M.C., 2009. First archeointensity results from Portuguese potteries (1550–1750 AD), *Earth Planets Space,* **61,** 93–100.

Hildenbrand, A., Weis, D., Madureira, P. & Marques, F.O., 2014. Recent plate re-organization at the Azores Triple Junction: evidence from combined geochemical and geochronological data on Faial, S. Jorge and Terceira volcanic islands, *Lithos,* **210–211,** 27–39.

Hill, M.J. & Shaw, J., 1999. Palaeointensity results for historic lavas from Mt Etna using microwave demagnetization/remagnetization in a modified Thellier-type experiment, *Geophys. J. Int.,* **139,** 583–590.

Hill, M.J. & Shaw, J., 2000. Magnetic field intensity study of the 1960 Kilauea lava flow, Hawaii, using the microwave palaeointensity technique, *Geophys. J. Int.,* **142,** 487–504.

Jackson, A., Jonkers, A.R.T. & Walker, M.R., 2000. Four centuries of geomagnetic secular variation from historical records, *Phil. Trans. R. Soc, A,* **358,** 957–990.

Kissel, C. & Laj, C., 2004. Improvements in procedure and paleointensity selection criteria (PICRIT-03) for Thellier and Thellier determinations: application to Hawaiian basaltic long cores, *Phys. Earth planet. Inter.,* **147,** 155–169.

Kruiver, P.P., Kok, Y.S., Dekkers, M.J., Langereis, C.G. & Laj, C., 1999. A pseudo-Thellier relative palaeointensity record, and rock magnetic and geochemical parameters in relation to climate during the last 276 kyr in the Azores region, *Geophys. J. Int.,* **136,** 757–770.

Leonhardt, R., Heunemann, C. & Krasa, D., 2004. Analyzing absolute paleointensity determinations: acceptance criteria and the software ThellierTool 4.0, *Geochem. Geophys. Geosyst.,* **5,** Q12016, doi:10.1029/2004GC000807.

Madeira, J., 2005. The volcanoes of Azores island: a world-class heritage (examples from Terceira, Pico and Faial Islands), in *Proceedings of the IV Internacional Symposium ProGEO on the Conservation of the Geological Heritage Field Trip Book,* European Association for the Conservation of the Geological Heritage and Centro de Geociências da Universidade do Minho, Braga.

Mitra, R., Tauxe, L. & McIntosh, S.K., 2013. Two thousand years of archeointensity from West Africa, *Earth planet. Sci. Lett.,* **364,** 123–133.

Monster, M.W.L., de Groot, L.V. & Dekkers, M.J., 2015. MSP-Tool: a VBA-based software tool for the analysis of multispecimen paleointensity data, *Front. Earth Sci.* **3,** 86, doi:10.3389/fearth.2015.00086.

Nachasova, I.E. & Burakov, K.S., 2009. Variation of the intensity of the Earth's magnetic field in Portugal in the 1st millennium BC, *Izv-Phys Solid Earth,* **45,** 595–603.

Nilsson, A., Holme, R., Korte, M., Suttie, N. & Hill, M., 2014. Reconstructing Holocene geomagnetic field variation: new methods, models and implications, *Geophys. J. Int.,* **198,** 229–248.

Paterson, G.A., Tauxe, L., Biggin, A.J., Shaar, R. & Jonestrask, L.C., 2014. On improving the selection of Thellier-type paleointensity data, *Geochem. Geophys. Geosyst.,* **15,** 1180–1192.

Paterson, G.A., Biggin, A.J., Hodgson, E. & Hill, M.J., 2015. Thellier-type paleointensity data from multidomain specimens, *Phys. Earth planet. Inter.,* **245,** 117–133.

Pavón-Carrasco, F.J., Osete, M.L., Torta, J.M. & De Santis, A., 2014. A geomagnetic field model for the Holocene based on archaeomagnetic and lava flow data, *Earth planet. Sci. Lett.,* **388,** 98–109.

Petrovský, E. & Kapička, A., 2006. On determination of the Curie point from thermomagnetic curves, *J. geophys. Res.-Solid Earth,* **111,** doi:10.1029/2006jb004507.

Pimentel, A., Zanon, V., de Groot, L.V., Hipólito, A., Di Chiara, A. & Self, S., 2016. Stress-induced comenditic trachyte effusion triggered by trachybasalt intrusion: multidisciplinary study of the 1761 AD eruption at Terceira Island (Azores), *Bull. Volcanol.,* **78**(3), 22, doi:10.1007/s00445-016-1015-6.

Quartau, R., Hipólito, A., Romagnoli, C., Casalbore, D., Madeira, J., Tempera, F., Roque, C. & Chiocci, F.L., 2014. The morphology of insular shelves as a key for understanding the geological evolution of volcanic islands: insights from Terceira Island (Azores), *Geochem. Geophys. Geosyst.,* **15,** 1801–1826.

Reimer, P.J. *et al.*, 2013. IntCal13 and Marine13 radiocarbon age calibration curves 0–50,000 years cal BP, *Radiocarbon,* **55,** 1869–1887.

Riisager, P. & Riisager, J., 2001. Detecting multidomain magnetic grains in Thellier palaeointensity experiments, *Phys. Earth planet. Inter.,* **125,** 111–117.

Self, S., 1976. The recent volcanology of Terceira, Azores, *J. Geol. Soc.,* **132,** 645–666.

Selkin, P.A. & Tauxe, L., 2000. Long-term variations in palaeointensity, *Phil. Trans. R. Soc, A,* **358,** 1065–1088.

Shaar, R., Ron, H., Tauxe, L., Kessel, R. & Agnon, A., 2011. Paleomagnetic field intensity derived from non-SD: testing the Thellier IZZI technique on MD slag and a new bootstrap procedure, *Earth planet. Sci. Lett.,* **310,** 213–224.

Stuiver, M. & Reimer, P.J., 1993. Extended ^{14}C data base and revised CALIB 3.0 ^{14}C age calibration program, *Radiocarbon,* **35,** 215–230.

Tauxe, L. & Staudigel, H., 2004. Strength of the geomagnetic field in the Cretaceous Normal Superchron: new data from submarine basaltic glass of the Troodos Ophiolite, *Geochem. Geophys. Geosyst.,* **5,** Q02H06, doi:10.1029/2003GC000635.

Tauxe, L., Pick, T. & Kok, Y., 1995. Relative paleointensity in sediments: a pseudo-Thellier approach, *Geophys. Res. Lett.,* **22,** 2885–2888.

Thellier, E. & Thellier, O., 1959. Sur l'intensité du champ magnétique terrestre dans le passé historique et géologique, *Ann. Geophys.,* **15,** 285–376.

Valet, J.-P., 2003. Time variations in geomagnetic intensity, *Rev. Geophys.,* **41,** 1004, doi:10.1029/2001RG000104.

Valet, J.-P. & Soler, V., 1999. Magnetic anomalies of lava fields in the Canary islands. Possible consequences for paleomagnetic records, *Phys. Earth planet. Inter.,* **115,** 109–118.

Vazquez, J.A. & Lidzbarski, M.I., 2012. High-resolution tephrochronology of the Wilson Creek Formation (Mono Lake, California) and Laschamp event using [238]U-[230]Th SIMS dating of accessory mineral rims, *Earth planet. Sci. Lett.,* **357–358,** 54–67.

Yu, Y. & Tauxe, L., 2005. Testing the IZZI protocol of geomagnetic field intensity determination, *Geochem. Geophys. Geosyst.,* **6,** Q05H17. doi:10.1029/2004GC000840.

Yu, Y., Dunlop, D.J. & Özdemir, Ö., 2003. Are ARM and TRM analogs? Thellier analysis of ARM and pseudo-Thellier analysis of TRM, *Earth planet. Sci. Lett.,* **205,** 325–336.

Zanon, V. & Pimentel, A., 2015. Spatio-temporal constraints on magma storage and ascent conditions in a transtensional tectonic setting: the case of the Terceira Island (Azores), *Am. Mineralog.,* **100,** 795–805.

SUPPORTING INFORMATION

Additional Supporting Information may be found in the online version of this paper:

Table S1. IZZI-Thellier results. Per site the details of the IZZI-Thellier interpretations are given, if three or more samples passed one or more sets of selection criteria as specified in the first (grey) rows of the table, the results are averaged, its standard deviation (*SD*) is specified and the *SD* is expressed as a percentage of the mean (must be <20 per cent to accept the estimate) below the black line, furthermore the 95 per cent confidence interval is given (95 per cent CI). Per sample the following parameters are specified: Site, sample number, lab field used, the obtained palaeointensity, the selection criteria passed, the 1σ of the palaeointensity estimate (Stddev), the minimum (T_{min}) and maximum (T_{max}) temperatures interpreted, the number of data points interpreted (*N*), the fraction of σ over the intensity (β), the fraction of the NRM interpreted (*f*), the gap factor (*g*), the quality factor (*q*), the fixed mean angular deviation (MAD), the angle between the floating and origin-anchored linear fits through the Zijderveld diagrams (α), the cumulative check error (CK-error), the maximum absolute difference produced by a pTRM check, normalized by the total TRM (CK-diff), the maximum difference ratio for the pTRM-checks (Drat), the extent of a pTRM tail after correction for angular dependence [d(t*)], the maximum absolute difference produced by a pTRM tail check, normalized by the NRM [d(TR)], and the maximum difference ratio for the tail-checks (Drat-tail).

Table S2. Pseudo-Thellier results at specimen level. All pseudo-Thellier results obtained in this study are specified, grouped per age. If more than three samples pass the selection criterion ($B_{\frac{1}{2}ARM}$ between 23 and 63 mT) the pseudo-Thellier slopes are averaged and specified together with its standard deviation (*SD*) and 95 per cent confidence interval (95 per cent CI) below the line.; also the number of accepted samples is expressed as fraction of the number of samples measured, and the standard deviation is expressed as a percentage of the mean. Per sample the following parameters are given: age, site, sample number, the absolute pseudo-Thellier slope (pTh slope), the field that imparts half of the full ARM ($B_{\frac{1}{2}ARM}$), the range of AF fields interpreted (AF-segm.), the NRM and saturated ARM magnetizations, and possible remarks. Samples that are rejected or do not pass the selection criterion are in red.
(http://gji.oxfordjournals.org/lookup/suppl/doi:10.1093/gji/ggw095/-/DC1).

Please note: Oxford University Press is not responsible for the content or functionality of any supporting materials supplied by the authors. Any queries (other than missing material) should be directed to the corresponding author for the paper.